7-1-1999

Diabatic Effects on Late-Winter Cold Front Evolution: Conceptual and Numerical Model Evaluations

William A. Gallus Jr.
Iowa State University, wgallus@iastate.edu

Moti Segal
Iowa State University

Diabatic Effects on Late-Winter Cold Front Evolution: Conceptual and Numerical Model Evaluations

Abstract

The impact of diabatic heating on late winter frontogenesis is evaluated both through conceptual scaling and the use of high-resolution Eta Model simulations of a strong but relatively dry cold surface front that occurred during the Storm-scale Operational Research Meteorology Fronts Experiment Systems Test (STORMFEST) project. Although skies were clear ahead of the front, it was trailed by an extensive area of cloud cover that influenced frontal strength during the daylight hours by reducing solar insolation and sensible heat flux.

An Eta control simulation of the event agreed reasonably well with observations and indicated intensification of the frontal temperature gradient during the daytime with a weakening at night. Additional simulations have been done to investigate sensitivity to several diabatic processes. These tests include the role of cloud shading on surface sensible heat flux, the role of soil moisture in the warm sector, and the role of evaporative cooling of precipitation in the light precipitation area behind the cold front. All of these diabatic processes have a measurable impact on the front, although soil moisture and cloud shading appear to play the most important roles. The moisture and static stability of the frontal environment were unfavorable for precipitation along the front, and the increase in frontal strength due to reduced surface sensible heat flux from extensive cloud shading behind the front did not significantly influence near-front precipitation for this event.

Disciplines

Meteorology

Comments

This article is published as Gallus Jr, William A., and Moti Segal. "Diabatic effects on late-winter cold front evolution: Conceptual and numerical model evaluations." *Monthly Weather Review* 127, no. 7 (1999): 1518-1537. DOI: 10.1175/1520-0493(1999)127<1518:DEOLWC>2.0.CO;2. Posted with permission.

Diabatic Effects on Late-Winter Cold Front Evolution: Conceptual and Numerical Model Evaluations

WILLIAM A. GALLUS JR.

Department of Geological and Atmospheric Science, Iowa State University, Ames, Iowa

MOTI SEGAL

Department of Agronomy, Iowa State University, Ames, Iowa

(Manuscript received 20 April 1998, in final form 1 July 1998)

ABSTRACT

The impact of diabatic heating on late winter frontogenesis is evaluated both through conceptual scaling and the use of high-resolution Eta Model simulations of a strong but relatively dry cold surface front that occurred during the Storm-scale Operational Research Meteorology Fronts Experiment Systems Test (STORMFEST) project. Although skies were clear ahead of the front, it was trailed by an extensive area of cloud cover that influenced frontal strength during the daylight hours by reducing solar insolation and sensible heat flux.

An Eta control simulation of the event agreed reasonably well with observations and indicated intensification of the frontal temperature gradient during the daytime with a weakening at night. Additional simulations have been done to investigate sensitivity to several diabatic processes. These tests include the role of cloud shading on surface sensible heat flux, the role of soil moisture in the warm sector, and the role of evaporative cooling of precipitation in the light precipitation area behind the cold front. All of these diabatic processes have a measurable impact on the front, although soil moisture and cloud shading appear to play the most important roles. The moisture and static stability of the frontal environment were unfavorable for precipitation along the front, and the increase in frontal strength due to reduced surface sensible heat flux from extensive cloud shading behind the front did not significantly influence near-front precipitation for this event.

1. Introduction

Late winter cold front activity is common in midlatitudes and important in forecasting considerations. A large number of studies have evaluated various aspects of these fronts. However, only a small amount of research attention has been given to the impact of diabatic processes on the characteristics of such fronts, particularly the intercomparison of their relative significance.

Variations in solar irradiance modify the surface sensible heat flux, which can in turn change the frontal temperature gradient. These effects may be induced by differential cloud cover near the front reducing solar irradiance reaching the surface (e.g., Businger et al. 1991; Koch et al. 1995; Segal et al. 1993; Miller et al. 1996; Blumen et al. 1996). Cloud cover confined primarily to the cold side of a front reduces solar irradiance reaching the surface there, consequently reducing sensible heat flux and enhancing the cross-front temperature gradient.

Surface wetness on the warm side of a front likewise affects the cross-front temperature gradient. It is worth noting that the change of the dewpoint temperature for a change in specific humidity is larger the lower the temperature. Therefore, though in late winter the evapotranspiration on warm days is relatively small compared to summer, its impact on the dewpoint might be larger, and correspondingly support low cloud formation. Increased surface wetness results in a decrease in the daytime temperature gradient and its related dynamical effects (Segal et al. 1993; Koch et al. 1997); however, the increased surface wetness will likely enhance thermodynamic forcing [see De Ridder (1997) and references therein] in the frontal warm sector. Koch et al. (1997) found that a reduction of soil wetness in the warm sector ahead of a cold front in a simulated spring case increased the precipitation due to a corresponding intensification of the front's dynamical effects (i.e., convergence). There may be an optimal surface wetness that maximizes both available soil moisture for cloud formation and the low-level convergence that enables the development of a favorable convective environment. The role

Corresponding author address: Dr. William A. Gallus, Department of Geological and Atmospheric Science, Iowa State University, 3025 Agronomy Hall, Ames, IA 50011.
E-mail: wgallus@iastate.edu

of surface wetness may be further complicated by the role of soil moisture outside the local region where precipitation forms, where surface effects might influence low-level moisture transport. Additional sensitivity simulations would be needed in order to evaluate the interrelationship between surface wetness and cold front potential rainfall activity. Likewise an attempt to generalize this interrelationship based on a conceptual model accounting for the main forcing would be useful.

Diabatic cooling from evaporation of precipitation, as well as melting of precipitation, can yield substantial dynamical forcing (e.g., Lin and Stewart 1991). The timescale in which diabatic effects can become significant is much shorter than that for the effects driven by solar radiation. It is of merit to compare these two types of diabatic effects as related to frontal processes.

In late winter and early spring, the above effects can play a significant role in frontal evolution. (Occasionally the diabatic effect of snowcover may be of importance.) During this period of the year, a latitudinal variability in solar irradiance and sensible heat flux forcing is likely. The frontal system of 9 March 1992 that passed through the dense observational network established over the central United States for the Storm-scale Operational Research Meteorology Fronts Experiment Systems Test (STORMFEST) provides an example of such a situation. As such, various aspects of the system have been evaluated in several studies including Martin et al. (1995), Wang et al. (1995), Miller et al. (1996), and Blumen et al. (1996). In the study of Wang et al., a standard diagnostic evaluation of the frontal event was suggested, but no details of the relative importance of the various diabatic processes maintaining the front were provided. The Miller et al. and Blumen et al. studies consist of observational analysis and the use of an analytic model designed to elaborate on the cloud shading thermal effect, while emphasizing surface temperature related frontal characteristics. The accumulation of research documentation for this cold front event provides an advantage in adopting this case for addressing additional issues related to late winter cold fronts.

The goal of the present study is to focus on this frontal case and to explore the impact of the previously described diabatic effects and their interrelationships on the development of the frontal system. First, a conceptual evaluation will be provided focusing on midlatitude late winter cold fronts. It attempts to provide scaling of basic properties of the diabatic effects. Next, a high-resolution version of the National Centers for Environmental Prediction (NCEP) Eta Model (e.g., Mesinger et al. 1988; Janjic 1994) is used to simulate the observed event, using the improved land surface scheme implemented in the operational model in 1997 (Chen et al. 1996). This control case is then compared with various simulations designed to explore sensitivity of the frontal structure to diabatic heating. The simulations address the effects of cloud shading, surface wetness, and evaporative cooling of the postfrontal rain. (Latent heating from condensation also was addressed but a simulation without it yielded unrealistic results, and therefore is not discussed.) In addition, some attention is given to evaluate the thermodynamic effect versus the dynamic effect on frontal precipitation. An attempt is made to generalize the results.

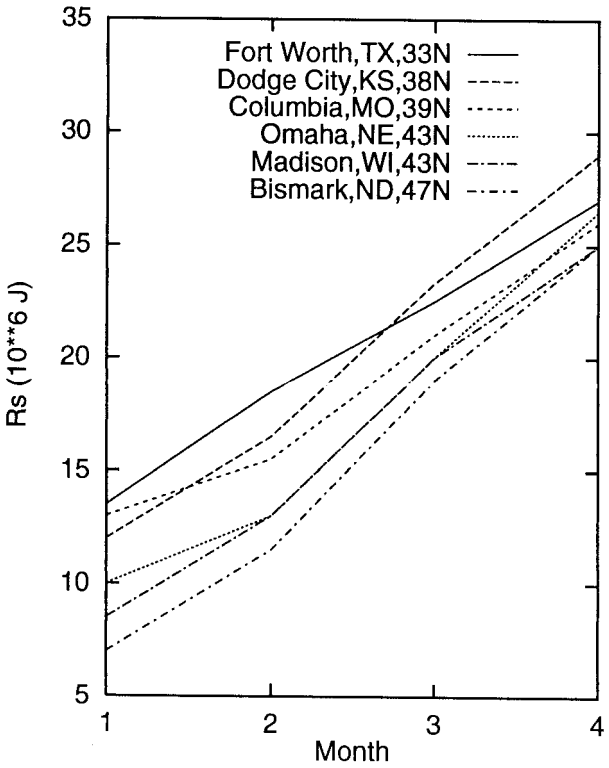

FIG. 1. Observed daily global solar irradiance on a horizontal surface (10^6 J m^{-2}) for the months Jan–Apr at the indicated sites. Based on U.S. Department of Energy (1981).

2. Conceptual evaluation of diabatic-related effects on late winter cold fronts

To enhance the insight into the mechanism and the significance of the diabatic forcing associated with late winter fronts, we provide the following conceptual evaluation. Additionally, we describe frontal evolution functions that are used later in the analysis of the model results.

a. Surface thermal fluxes affecting frontal temperature gradient

1) SOLAR RADIATION EFFECTS

The impact of cloud shading or soil wetness on differential sensible heat flux–forced temperature gradients (gradients modified by particular spatial distributions of heat fluxes) is proportional to the magnitude of solar irradiance, and is therefore related to the solar day of the year. Figure 1 illustrates the daily observed clear

sky global solar irradiance for the winter–early spring period at various midlatitude sites in the central United States. The daily values of solar irradiance range from $\sim 10 \times 10^6$ J m^{-2} in mid-January to $\sim 25 \times 10^6$ J m^{-2} in mid-April with a noticeable latitudinal dependence in midwinter. (For comparison purposes, the mid-June value is $\sim 31 \times 10^6$ J m^{-2}.) The fraction of the solar irradiance contributing to sensible heat flux, η, depends on the Bowen ratio (ratio of sensible heat flux to latent heat flux), and it is most commonly in the range 0.1–10 (corresponding to a range from very wet to dry surfaces). The impact of daytime sensible heat flux on the frontal temperature gradient is confined to the depth of the winter convective boundary layer (WCBL), which is likely to be relatively shallow compared to that in the summer. The most pronounced effect is on temperature near the surface, with effects diminishing almost linearly to zero at the top of the WCBL (Segal et al. 1993). This behavior has to be accounted for while making observational evaluations based on meteorological shelter temperature, as the shelter temperatures indicate cross-front gradients that are larger than the layer averaged temperature gradients. Using Fig. 1 and estimating η and the WCBL depth, one might scale the corresponding daytime increase in the average WCBL temperature. Adopting a WCBL depth of 1000 m and $\eta = 0.25$ (a mildly wet surface) as representative values, then for the January–March period the average daily temperature increase within the WCBL is 2.5°–5°C. This suggests that the solar radiation related diabatic effect for weak cold fronts would be relatively pronounced, whereas for intense cold fronts it would be of less significance.

The solar irradiance contribution to sensible heat flux in the cold side of the front, when this region experiences overcast conditions, is of secondary magnitude regardless of the landscape characteristic of the surface. If the cloud cover is only partial or negligible the differential heating effect is reduced. When the warm sector area of the front consists of an extensive wet or snow-covered surface, the contribution of solar radiation to the thermal gradient of the front would tend to be reduced.

2) LONGWAVE RADIATION EFFECTS

Cloud cover over the cold sector would increase incoming longwave radiation (LWR) at the surface. For dense overcast consisting of low-level clouds the increase might be as high as 20%. For a relatively high value of incoming LWR ($\sim$300 W m^{-2}) the increase at the surface would be 60 W m^{-2} and associated with about half of the magnitude of increase in the LWR flux divergence within the layer between the cloud base and the surface (Ye et al. 1989). This diabatic influence might have a secondary effect of reduction of the cold front thermal contrast for the entire cold front sector volume, mostly when deep cold fronts are considered. However, its impact on the shelter temperature might be significant. Ye et al. (1989) estimated cloud radiative effects on the nocturnal minimum shelter temperature based on numerical modeling and observations, and suggested an increase in the range 2°–10°C compared with clear sky cases. Thus, for deep cold fronts with cloud cover constrained to the cold sector one should consider that shelter temperature observations might underestimate frontal intensity.

3) SOIL HEAT STORAGE EFFECTS

Unlike spring and summer, in late winter a large portion of the midlatitudes consists of bare soil. Sanders (1955) pointed out that post-cold-frontal increases in sensible heat flux, H_s, act to reduce the frontal temperature gradients. Apparently no attempts have been made to quantify this effect. The passage of the cold front effectively generates a heat storage in the upper soil layer relative to the postfrontal cooler atmosphere. For scaling purposes it is reasonable to assume that (i) the involved soil layer depth, h_s, is roughly the layer affected by the diurnal change of temperature (typically in the late winter, h_s values are 0.1–0.3 m), (ii) the apparent temperature increase of the effectively generated soil thermal storage is $\Delta T/2$, where ΔT is the increase in the difference between the air and soil surface temperature immediately following the passage of the front. (For scaling purposes ΔT is equivalent to the front's warm–cold sector air temperature difference.) The magnitude of the effectively generated soil thermal storage, S_T, can be estimated as $S_T = \rho_s c_s h_s \Delta T/2$, where ρ_s is the soil density and c_s is the soil specific heat. For illustration we adopt $h_s = 0.2$ m, $\Delta T = 15$°C (typical of the front evaluated later), and a range of ρ_s and c_s values as given in Garratt (1992, p. 291). For dry soil $S_T \cong 2 \times 10^6$ J m^{-2}, of which a large portion is converted into sensible heat flux. [It is worth noting that the estimated magnitude of S_T is smaller compared with the daily accumulated H_s estimated in section 2a(1).] For wet soil, $S_T \cong 4 \times 10^6$ J m^{-2}, however, a large portion of it would be consumed during the daytime by surface evaporation.

To provide initial quantification of the involved modifications in the surface values of H_s due to advection of cold air, eight simulations were performed using a 1D version of the Eta Model. The initial conditions resembled those described in section 3 for the warm sector of the simulated front. In seven simulations, 15°C drops in the atmospheric temperature were introduced at the times indicated in Fig. 2 to resemble the temperature changes occurring with passage of an intense cold front. In the simulations, daytime increases larger than 200 W m^{-2} were simulated immediately following the introduction of the temperature drop; however, the values declined gradually with time. The impact of daytime temperature on H_s is noticeably larger than the nighttime impact (Fig. 2). When a daytime temperature

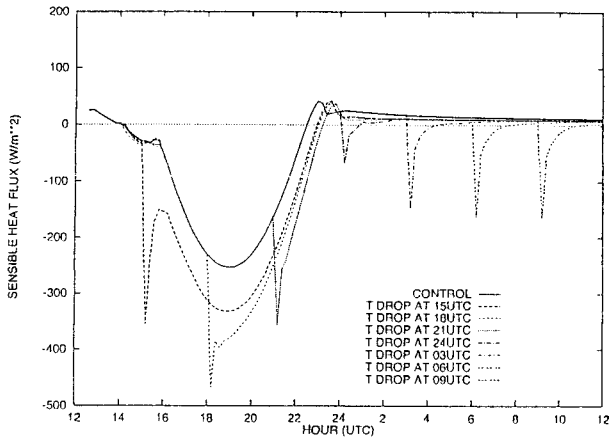

FIG. 2. Simulated diurnal sensible heat flux for the central United States in 1D Eta version in which the atmospheric temperature was dropped 15°C at the indicated times (except in the control run).

drop is associated with cloud shading, a sensible heat flux decrease is likely around midday. It is worth noting that H_s reached a peak of about 250 W m^{-2} in the control run; however, values may reach above 400 W m^{-2} for dry soil.

b. Precipitation evaporative cooling affecting cold sector temperature

The evaporation of precipitation (and likewise melting and sublimation) can result in significant cooling of portions of the troposphere and has been shown to influence frontal behavior (Oliver and Holzworth 1953). At least as early as 1945, Hamilton and Archbold (1945) showed that microphysical cooling played a major role in the development of mesoscale circulations associated with convective systems. Although the precipitation rates associated with late winter cold fronts may be much smaller than those associated with warm season convective systems, evaporative cooling can still be significant due to the magnitude of the latent heat of condensation. For instance, assuming relatively typical late winter values for temperature, 5°C, and relative humidity, 70%, the actual mixing ratio would be 1.8 g kg^{-1} lower than the saturation mixing ratio. The equation for evaporation of rainwater used in the microphysical model of Gallus and Johnson (1995) predicts a 0.6 g kg^{-1} h^{-1} increase in mixing ratio due to evaporation for a light rainfall rate (2 mm h^{-1}) with this relative humidity. The corresponding cooling rate would be 1.5°C h^{-1}. With no additional sources or sinks of heat or moisture, the temperature would eventually fall to its wet-bulb value, around 2°C. The total cooling from evaporation (3°C) would occur in a period of roughly 3 h. If these values were consistent in the WCBL, the cooling from evaporation would be the same magnitude as the warming from the enhanced surface sensible heat flux [see subsection 2a(1)]. During the warm season, convective outflow boundaries due in large part to the evaporation of rainfall often advance well ahead of cold fronts and become a more important forcing mechanism for precipitation than the actual front. Thus it should be expected and as supported by studies reviewed in Lin and Stewart (1991) that preferential rainfall evaporation on the cold side of a front will help to maintain the front intensity and possibly increase the cross-front vertical circulation.

c. Time evolution of frontogenesis, frontal convergence, and frontal moisture convergence

The modeling presented in this study enables sensitivity evaluations to be carried out utilizing expressions indicating temporal variations of the frontal thermal gradient, convergence, and moisture convergence. Of particular interest is the frontal evolution associated with daytime solar radiation related forcing, and its change with the transition into the nocturnal period. As the evaluations are made in this study in a cross-front direction, the expressions are formulated adopting two-dimensional symmetry. (As will be shown later, the temperature gradient in the case simulated by the model was primarily directed in the cross-front direction.) The frontogenesis-related functions $F(\cdot)$ reflect the temporal variation of the horizontal gradient in the property $(\cdot)$ at the location of the front. The functions take the form $F(\cdot) = (D/Dt)[(\partial/\partial x)(\cdot)]$, where x is the cross-front direction. Following Garratt and Physick (1987)

$$\frac{D}{Dt} = \frac{\partial}{\partial t} + c\frac{\partial}{\partial x}, \tag{1}$$

where c is the frontal speed of propagation. The value of $F(\cdot)$ is therefore evaluated at any given time at the frontal location.

The first frontogenesis function F_θ is related to the cross-front potential temperature gradient. It is a classical indicator of front strength introduced by Miller (1948) and has been used in many studies. Adopting Garratt and Physick (1987), its cross-front value is given by

$$F_\theta = \frac{D\theta_x}{Dt} = -u_x\theta_x - (\mathbf{V} - c\mathbf{i}) \cdot \nabla(\theta_x) - w_x\theta_x + Q_x, \tag{2}$$

where $\mathbf{V} = (u, w)$, $\nabla \equiv \mathbf{i}(\partial/\partial x) + \mathbf{k}(\partial/\partial z)$ with $\mathbf{i}$ and $\mathbf{k}$ unit vectors along x and z, c is the frontal speed, and Q is the diabatic heating rate (including microphysical and radiative effects). The first term on the rhs is related to horizontal convergence, the second relative advection, the third a tilting of isentropes from differential vertical motion, and the fourth differential diabatic heating. The diabatic heating in the model can be due to moist processes or radiation effects.

The second indicator F_u is related to temporal changes in the convergence across a front. It provides a direct

indication of lifting associated with the front (whereas F_θ provides only an indirect indicator of lifting intensity). Following Garratt and Physick (1987), F_u is given by

$$F_u = \frac{D(-u_x)}{Dt} = u_x u_x - (\mathbf{V} - c\mathbf{i}) \cdot \nabla(-u_x) + w_x u_x - f v_x + \frac{P_{xx}}{\rho} - F_{xz}, \quad (3)$$

where similar notation is used as in Eq. (2). The first term is related entirely to convergence, the second relative advection, the third tilting, the fourth Coriolis effects on the alongfront winds (f is the Coriolis parameter), the fifth changes in pressure gradient across the front, and the last term, friction. From considerations of the potential impact of frontogenesis on precipitation, F_u as an indicator of the time evolution of vertical motion should be seen as an improved indicator compared with F_θ.

As the most interesting evaluation of a cold front would be related to its impact on precipitation, we propose a more direct indicator on this process than those provided by Eqs. (2) and (3) above. As precipitation potential is related to moisture convergence $[(-uq)_x]$ at the frontal zone, we evaluate its temporal variation by introducing

$$F_{uq} = \frac{D[(-uq)_x]}{Dt} = q\frac{D(-u_x)}{Dt} - u_x\frac{Dq}{Dt} - q_x\frac{Du}{Dt} + uu_xq_x - u(\mathbf{V} - c\mathbf{i}) \cdot \nabla(q_x) + uw_xq_x - u\left(\frac{Dq}{Dt}\right)_x, \quad (4)$$

where the first term is related to temporal changes in convergence, the second to moistening or drying, the third to acceleration in u in the presence of a moisture gradient, the fourth to convergence acting in a moisture gradient, the fifth to relative advection, the sixth to tilting, and the last term to differential moistening or drying across the front.

3. Model configuration and initial conditions

To investigate the influence of several diabatic processes on the frontal evolution of the 9 March case, a high-resolution workstation version of the NCEP Eta Model was used. The Eta Model was chosen because it is currently the primary short-range forecasting model used operationally in the United States, and the land surface physics were markedly improved in 1997 with the inclusion of a modified Oregon State University (OSU) parameterization essentially similar to the Noilhan and Planton (1989) scheme, which captures the main biophysical controls on evapotranspiration (these processes would be mostly pertinent in the warmer section of the simulated domain). It was felt that the land surface parameterization of the model could reasonably simulate the important processes for this case. Multiple 1D, 2D, and 3D sensitivity experiments with the model suggested no significant weaknesses in the model's ability to simulate surface exchange processes important in this event.

The moist physics in the model include the modified Betts–Miller–Janjic convective parameterization (Betts 1986; Betts and Miller 1986; Janjic 1994) with both shallow and deep convection, and an explicit cloud water parameterization (Zhao 1991). Vertical turbulent exchange is calculated based on the Mellor–Yamada level 2.5 model (Mellor and Yamada 1974, 1982) with some recent modifications (Lobocki 1993; Gerrity et al. 1994). A seven-layer version of the modified OSU soil model (e.g., Pan and Mahrt 1987; Holtslag and Ek 1996) with a vegetation canopy is used for land surface physics. Soil moisture and temperature are explicitly forecast for the seven soil layers along with a surface skin temperature. Evapotranspiration comprises three components, including direct evaporation from the soil surface, direct evaporation from wet vegetation (of intercepted rain or dew), and transpiration from the vegetation canopy.

Three-dimensional runs were performed with 22-km horizontal resolution in a roughly 2000 km × 2000 km domain centered on the midwestern United States (see Fig. 4a). Vertical resolution generally varied from around 125 m in the lowest of 32 model layers to around 1 km at model top. Initial and boundary data for the simulations were supplied from 40-km data taken from a prior 48-km Eta run initialized at 0000 UTC 9 March 1992. Integrations were carried out for 36 h. (Following this period the front began to interact with ongoing convective activity in the southeastern portion of the domain.)

The synoptic setting at the time of initialization can be seen in Fig. 3a. At that time, an intense surface low (994 mb) was centered in eastern Colorado with an extensive area of precipitation to its north and eastward along and behind a slow-moving cold front that extended east-northeast into Iowa and Wisconsin. [More extensive description of the synoptic pattern can be found in Martin et al. (1995), Wang et al. (1995), and Miller et al. (1996).] In the warm sector to the south of the front, scattered intense convection was occurring. Unseasonably warm temperatures covered most areas south of the front (generally 16°–22°C), with temperatures falling to around 0°C in northern Minnesota, North Dakota, western South Dakota, and westward. Soils were generally unfrozen across the domain, with the 0°C soil temperature line (not shown) located around the 0°C air temperature contour at 0000 UTC. In spite of the relatively high temperatures in the warm sector, the growing season had not yet begun in most areas and vegetation was absent or dormant in all areas north of

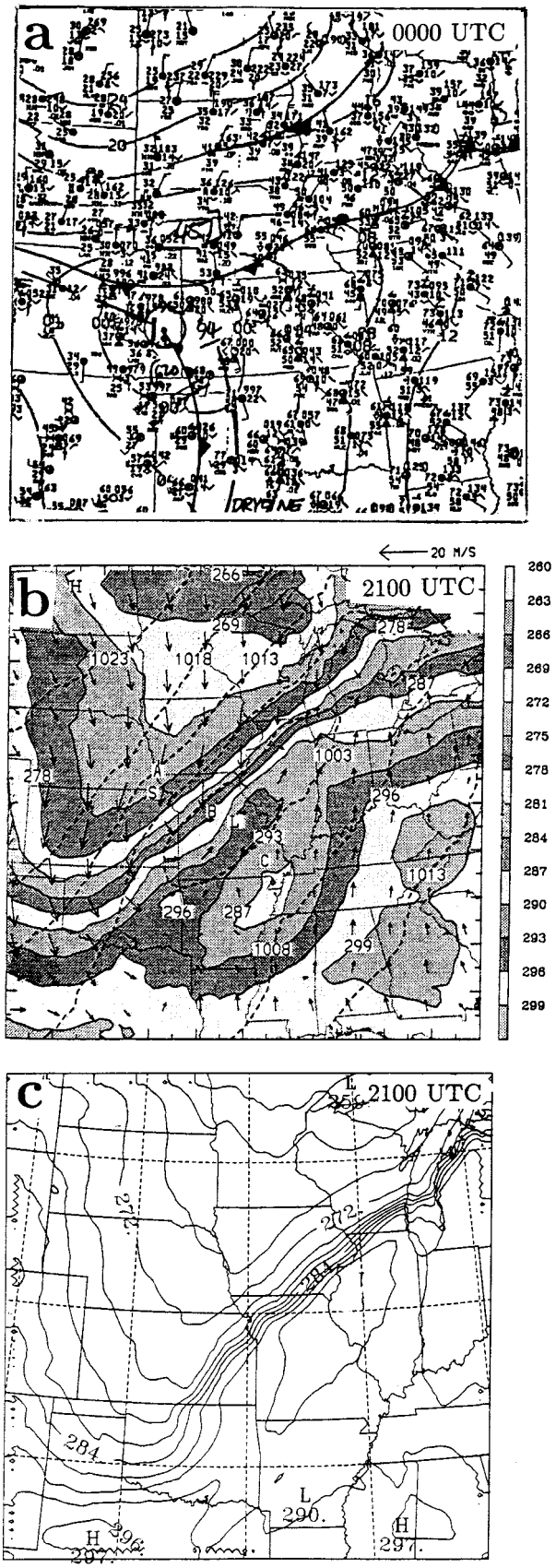

Texas and Louisiana. Thus, evapotranspiration would be similar in much of the domain to that associated with bare soil.

Initial soil moisture and temperature data were taken from the NCEP archived data for this case, and interpolated from the original two layers to the seven layers used in the high-resolution version of the model. Gridded fields of 8 soil types and 12 vegetation types were determined from Environmental Protection Agency and United Nations Food and Agriculture Organization datasets, respectively. Topography data were provided from a 30-s United States Geological Survey dataset. Vegetation fraction in the model was prescribed based on vegetation type and latitude.

A control simulation (CTL) was run for the event using the above model configuration and initialization. In addition, three sensitivity tests were performed to evaluate the effects of cloud shading, soil wetness, and evaporation of precipitation on the frontal evolution (see Table 1).

4. Control simulation

a. Propagation and evolution of cross-front temperature gradients

The control simulation addresses several objectives: (i) validating that general observed features related to the front are resolved, (ii) analysis of several forcing processes related to the front, and (iii) establishing a reference case for comparison with sensitivity simulations.

The 22-km version of the Eta Model simulated the 9 March cold front well, with results agreeing closely with available observations. An intense cyclone, with a closed circulation through 500 mb, gradually moved east-northeastward and weakened during the simulation. As mentioned above, a cold front extending northeast from the surface cyclone (Fig. 3a) was located across portions of Nebraska, Iowa, and Wisconsin at the start of the integration (0000 UTC). Observations showed that the surface low pressure system had weakened slightly by 2100 UTC (Fig. 3b) as it moved into Missouri. The front accelerated somewhat during the daytime hours (1500–2100 UTC) and the potential temperature gradient intensified (Miller et al. 1996). At 2100 UTC, the leading edge of the cold air [determined by Miller et al. (1996) to approximately follow the 287-

←

FIG. 3. Observations of the front on 9 Mar 1992 at (a) 0000 UTC and (b) 2100 UTC. (a) Standard station plotting procedure is used with standard frontal notation and pressure contoured with a 4-mb interval. (b) From Miller et al. (1996), potential temperature (K) is shaded (grayscale following label at right) with solid contours (every 3 K) and pressure is overlaid with dashed contours (5-mb interval). Ground-relative vector winds are scaled by the arrow above the upper-right corner. (c) Simulated potential temperature (contour interval 3 K) is shown at 2100 UTC.

TABLE 1. Description of the Eta simulations for 9–10 Mar 1992.

Simulation	Description
CTL	Control run for 9–10 Mar 1992
RAD	As in CTL, however without cloud effects on radiation
DRY	As in CTL, however with a 50% decrease in volumetric soil moisture
EVP	As in CTL, however without evaporative cooling of precipitation

K contour] was located from southeastern Kansas northeastward across extreme northeastern Missouri, northwestern Illinois, and into Lake Michigan just north of Chicago.

A comparison of the potential temperature observations at 2100 UTC (Fig. 3b) with the simulated potential temperature field at 2100 UTC (Fig. 3c) shows that the model simulated the general patterns well. Simulated potential temperatures in the northern plains, however, were up to a few degrees Celsius lower than observed. It is possible that a small overestimate of cyclone intensity in the model may have resulted in greater cold air advection than observed here. The model did depict the band of increased warmth ahead of the front, but with a weakness in the southern part of the domain. Some of the small-scale differences in this region may be due to location errors of simulated convective cloud cover. The model clearly shows the front with a sharp θ contrast. The simulated frontal speed was slightly underestimated, particularly in the northeastern part of the domain. The simulated cold front appears to lie up to 50–100 km northwest of the observed front. More detailed observations in Miller et al. (1996) imply that the model was already somewhat slow with the frontal position at 1200 UTC. Simulated mean sea level pressures (not shown) agreed well with observations, with the model cyclone only 1–2 mb deeper than that observed. However, the region of lowest pressure extended farther northeast in the model, and the increased southerly flow in this region may have retarded the movement of the front there.

During the first 12 h of the simulation, the front moved slowly southeastward at 5 m s^{-1} or less, extending from a surface low in central Kansas into extreme southeastern Nebraska, eastern Iowa, and into southeastern Wisconsin at 1200 UTC (see Fig. 4a). Significant precipitation occurred during these first 12 h along and north of the front (not shown). During the daylight hours of 9 March, the front continued to move southeastward, and the surface temperature (approximated using the lowest model layer ~70 m) gradient along the front intensified. Whereas the peak temperature change over a roughly 100 km distance was 13°C at 1200 UTC, it reached 15°C at 1800 UTC (Fig. 4b) and peaked at around 17°C at 0000 UTC 10 March (Fig. 4c). After sunset, the gradient rapidly weakened, and by 0600 UTC, the peak change over a 100-km distance was no more than 14°C (Fig. 4d). The western portion of the front, passing through Kansas and Oklahoma accelerated to around 13 m s^{-1} as it moved southeastward between 1800 UTC 9 March and 0600 UTC 10 March. The weakening of this portion of the front may have been assisted by large-scale frontolysis as the surface low weakened and moved well to the northeast of this region, or by topographic effects. Frontal movement farther east accelerated to 8–10 m s^{-1} toward the southeast.

The diurnal cycle in frontal temperature gradient intensity was also shown in the observational studies of this case (see Miller et al. 1996; Blumen et al. 1996). Using hourly surface observations spaced 100–115 km apart, the frontal gradient was shown to peak in the mid to late afternoon hours with a gradient of roughly 10°C $(100\ km)^{-1}$. (Much higher-resolution aircraft observations, reported in Miller et al., found the gradient peaked around sunset at 8°C km^{-1}.)

The depth of the front (implied by the temperature gradient) also appeared to increase from 1200 UTC (Fig. 5a) to 0000 UTC (Fig. 5b). The vertical cross sections shown in this figure were taken perpendicular to the front, generally from around Huron, South Dakota, to Quincy, Illinois, at 1200 UTC and from near Storm Lake, Iowa, to Dyersburg, Tennesee, at 0000 UTC (locations are marked in Figs. 4a and 4c, respectively). The strongest temperature gradient at 1200 UTC was about 1 km deep and oriented nearly vertically, although a significant gradient did extend to nearly 2.4 km and sloped rearward. By 0000 UTC, a strong temperature gradient extended up to around 1.6 km. The gradient was nearly vertical in the lowest 0.8 km, but sloped significantly above that level. Some increase in the temperature gradient occurred at all levels up to around 3.0 km.

Extensive cloud cover was observed in this event to be confined primarily to locations behind the cold front, or well ahead of it, with a broad zone (300–600-km wide) of relatively clear skies along and just ahead of the front [see Fig. 5 in Miller et al. (1996)]. The simulated field of shortwave radiation (without albedo affects) reaching the surface at 1600 UTC (Fig. 6a), 1800 UTC (Fig. 6b), and 2000 UTC (Fig. 6c) agrees rather well with the observations [Figs. 5, 17 in Miller et al. (1996); Fig. 2 in Blumen et al. (1996)]. Shortwave radiation was reduced significantly in a zone 300–500 km wide just behind the cold front (shown with a dashed line). No reduction was occurring in the clear region extending from Oklahoma northeastward into southeastern Iowa and parts of western Illinois. In the regions of thickest cloud cover, the shortwave radiation was reduced by over 80% from clear sky values. It can also

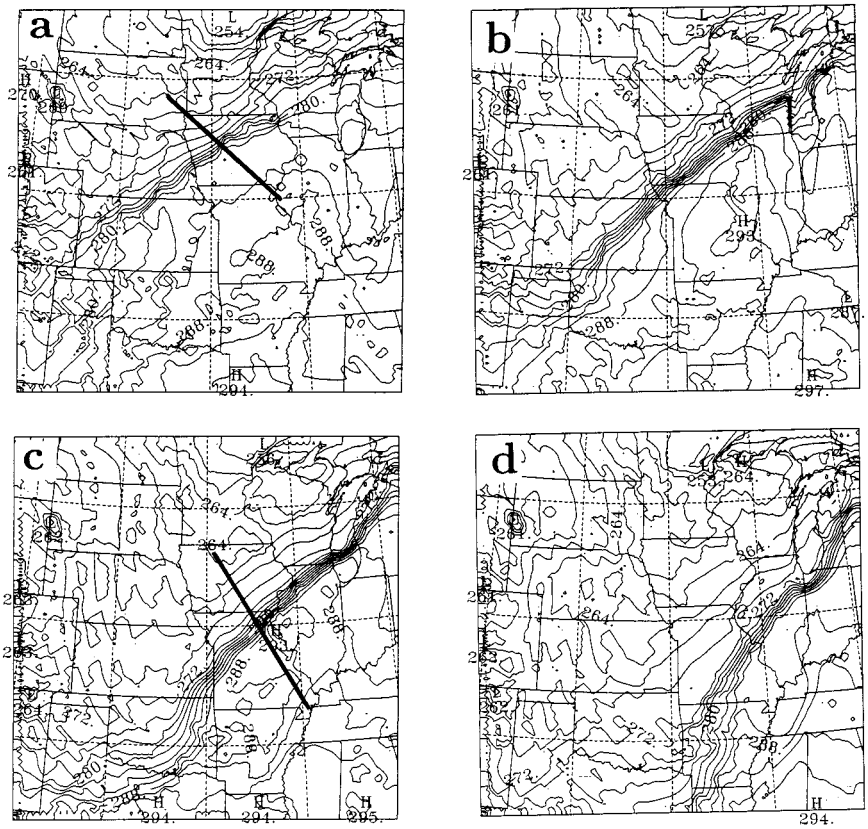

FIG. 4. Simulated surface temperature (lowest model layer, ~70 m) in K. Initialized at 0000 UTC 9 Mar and valid 9–10 Mar at (a) 1200 UTC, (b) 1800 UTC, (c) 0000 UTC, and (d) 0600 UTC. Contour interval is 2 K. Solid lines indicate the locations of cross sections shown in Fig. 5.

be seen in Fig. 6 that the reduction in simulated shortwave irradiance was gradual over a roughly 100-km distance behind the front. In addition, there were some small regions (generally less than 50 km wide) just behind the front, where skies were not yet cloudy. Although observations do suggest a weakness in the cloud cover in northwestern Missouri (Fig. 2 in Blumen et al. 1996) where the model was slowest to develop postfrontal clouds, cloudiness in general was observed in all regions behind the front. Taking into account the

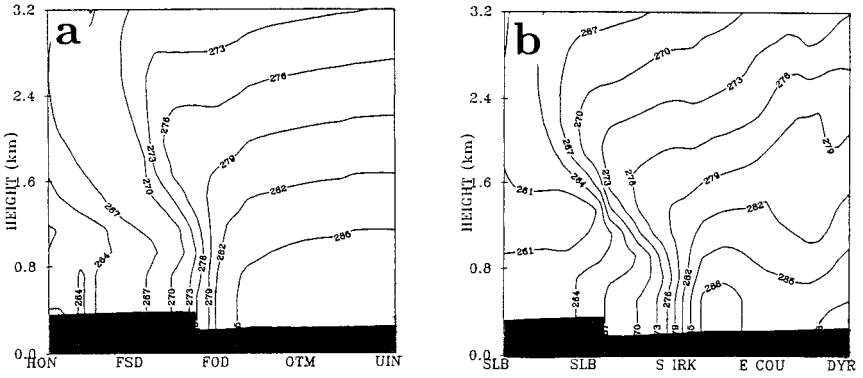

FIG. 5. Vertical cross section of temperature (K) through front at (a) 1200 UTC 9 Mar and (b) 0000 UTC 10 Mar. Contour interval is 3 K. Cross section at 1200 UTC is taken from near Huron, SD (HON), to Quincy, IL (UIN). Cross section at 0000 UTC is from near Storm Lake, IA (SLB), to Dyersburg, TN (DYR). The Eta step representation of topography in the cross section is indicated by the darkening. The location of the cross sections is indicated by a solid line in Figs. 4a and 4c, respectively.

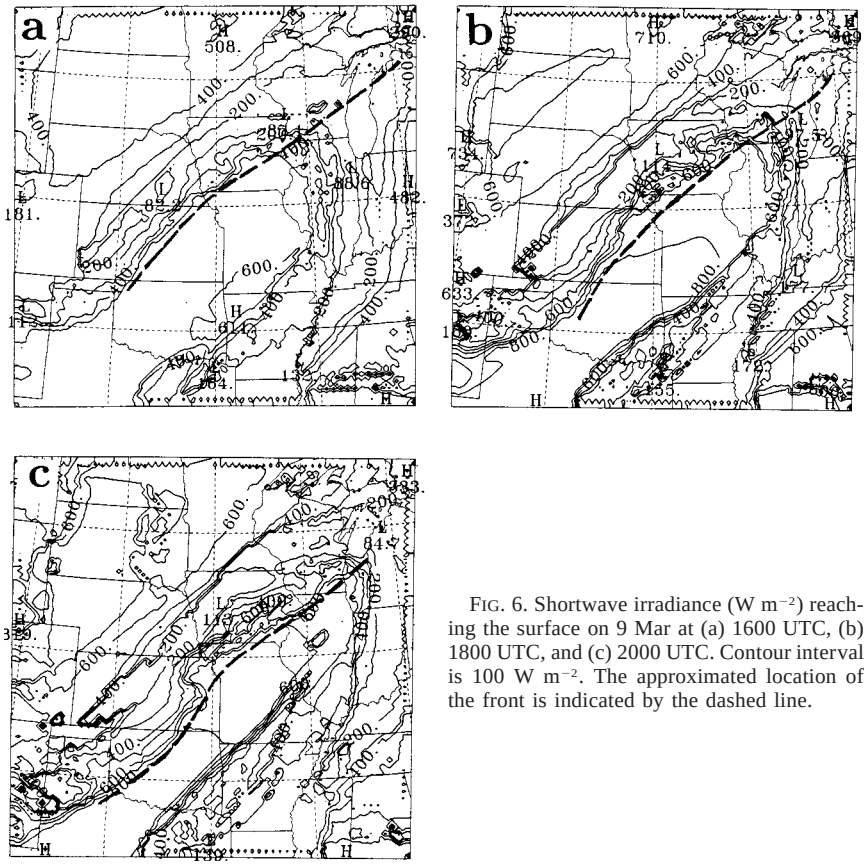

FIG. 6. Shortwave irradiance (W m^{-2}) reaching the surface on 9 Mar at (a) 1600 UTC, (b) 1800 UTC, and (c) 2000 UTC. Contour interval is 100 W m^{-2}. The approximated location of the front is indicated by the dashed line.

movement of the front, this difference between simulated and observed cloud cover would allow a few more hours of generally unobstructed shortwave irradiance to reach the surface at some points in the model (compared to observations) before the thick postfrontal cloud cover occurred.

b. Cross-front sensible and soil thermal fluxes

The combined effect of cross-front differential cloud cover and advection of cold air over a relatively warm surface resulted in significant gradients of surface sensible heat flux within the frontal zone during the daytime (Fig. 7a). Typical values in the Midwest at 2000 UTC in generally clear regions were around -70 to -140 W m^{-2} (negative sensible heat flux is directed upward). These rather low magnitudes reflect the wetness of the soil in this region on this date. Blumen et al. (1996) report even lower values observed for the midday hours from a Kansas site. The sensible heat flux did not vary in a simple fashion across the front. Immediately behind the front, cold air moved over a well-heated ground, and shortwave radiation had not been reduced at the surface as much as it had in regions over 100 km behind the front. Therefore, sensible heat flux increased strongly to magnitudes exceeding 280 W m^{-2} in this zone. Slightly farther behind the front, where thick cloud cover greatly reduced the incoming shortwave radiation and the ground had more time to cool, sensible heat fluxes decreased to values below 70 W m^{-2}. Thus, a gradient existed of around 210 W m^{-2} over a distance of around 200 km. This value is consistent with the 2–3-K cooling found to be attributable to cloud shading effects in a sensitivity test discussed later.

The modifications in the sensible heat flux correspond through the surface heat balance equation primarily to modifications in the surface soil and latent heat flux during the middle of the day and to soil heat flux alone at other times. The rapid drop in the air temperature behind the cold front as it passed some locations around midday resulted in significant gradients of the soil heat flux (Fig. 7b). At this time (2000 UTC), negative soil heat fluxes (directed downward) of 90–150 W m^{-2} were occurring ahead of the front. Shortly behind the front, these fluxes became positive with comparable magnitudes. Gradients as large as 200–250 W m^{-2} or more over a 100-km distance occurred along a large section of the front. These gradients were comparable to, or even exceeded, those found in the field of sensible heat flux.

During the night a strong gradient continued to exist in both the sensible (Fig. 7c) and soil (Fig. 7d) heat

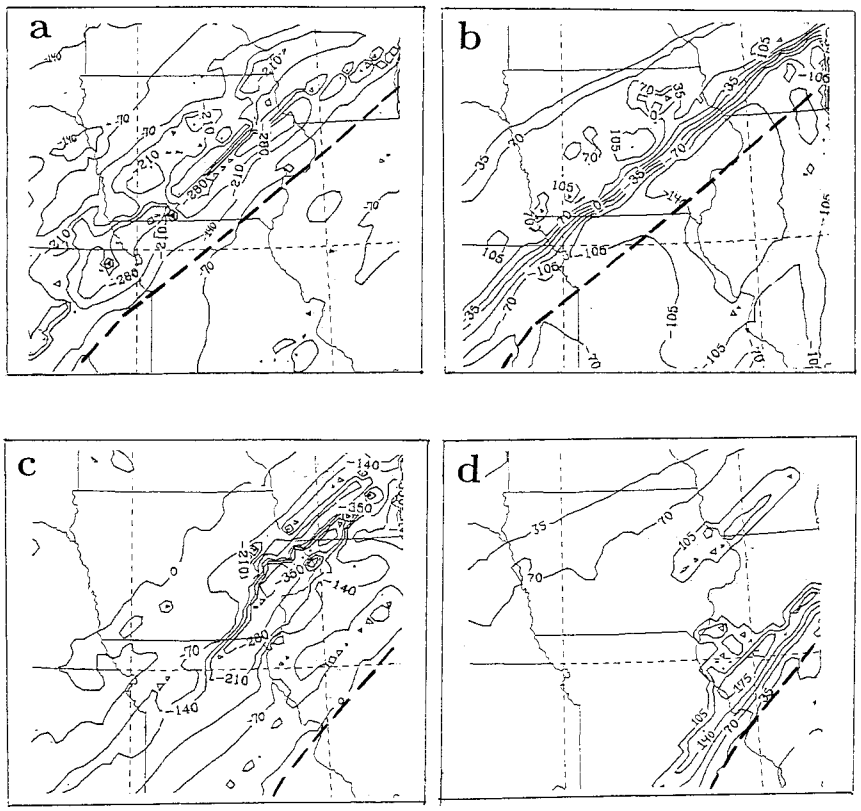

FIG. 7. Surface thermal fluxes across a well-developed portion of the front centered on Iowa and Missouri: (a) surface sensible heat flux at 2000 UTC, (b) surface soil flux at 2000 UTC, (c) same as in (a) except for 0600 UTC, (d) same as in (b) except for 0600 UTC. Contour interval is 70 W m^{-2} in (a) and (c) and 35 W m^{-2} in (b) and (d). The approximated location of the front is shown in each figure by a dashed line.

fluxes. Again, fluxes were largest in a region behind the cold front where the temperature contrast between the warmer ground and the air was greatest. The region of greatest sensible heat flux was located somewhat farther to the rear of the front at this time compared with 2000 UTC (Fig. 7a). This orientation of the maximum fluxes was frontolytic for nearly all of the frontal zone (region of significant temperature gradient) at this time. However, a rapid decrease in the fluxes farther to the northwest would provide a frontogenetic contribution well behind the cold front, and in portions of Iowa, this contribution exceeded that found during the daylight hours. The gradient in the soil fluxes was reduced slightly at 0600 UTC (Fig. 7d), with typical values near the front peaking at 150 W m^{-2} over a 100-km distance. The gradient in the soil fluxes was located immediately behind the front.

c. Precipitation

Simulated precipitation patterns (Fig. 8) are in reasonable agreement with observed patterns reported in Wang et al. (1995, Fig. 5). Although the temperature gradients associated with this front were significant, implying an intense frontal circulation (e.g., Miller 1948; Sawyer 1956; Eliassen 1962), most of the precipitation during the simulation occurred well to the north or the south of the 9 March daytime position of the front. Accumulated precipitation during 6-hourly intervals of 1200–1800 UTC and 1800–0000 UTC 9–10 March can be seen in Fig. 8. Convection just ahead of the front dissipated early in the simulation (prior to 0600 UTC 9 March). During the morning (1200–1800 UTC), significant precipitation occurred either well behind the front or deep in the warm sector in the southern Mississippi River valley (Fig. 8a). During the afternoon and evening, the model predicted only scattered light amounts closer to the front (Fig. 8b). Observations showed that the front remained relatively inactive. Simulated soundings in the warm sector showed relatively small amounts of convective available potential energy, as southwesterly surface winds limited the low-level moisture.

d. Time evolution of frontal temperature gradient (F_θ)

The observational studies of Miller et al. (1996) and Blumen et al. (1996) determined that a significant portion

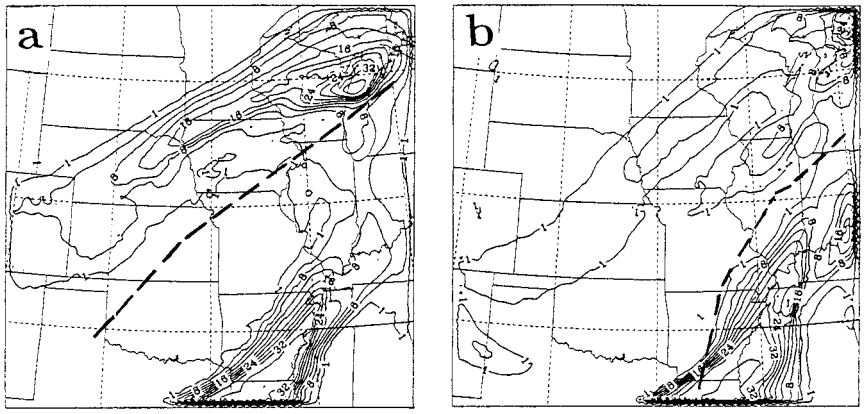

FIG. 8. Accumulated precipitation (mm) during 9–10 Mar for 6-hourly periods ending at (a) 1800 UTC and (b) 0000 UTC. Contours at 1 mm, and then with an interval of 4 mm below 32 mm, 8 mm above 32 mm. The approximated location of the front at the end of each 6-h period is shown by a dashed line.

of the frontogenesis (F_θ) during the daytime hours during this event was caused by the effect of cross-front gradients of diabatic warming associated with sensible heat transfer at low levels. The observations used to evaluate frontogenesis, however, were mostly restricted to the surface. Because this model run simulates the frontal evolution adequately, we have used a similar frontogenesis equation for temperature gradient [Eq. (2)], with model data to evaluate the temporal and vertical variation in frontogenesis. As Eq. (2) may be applied at any altitude within the front, to facilitate integrative evaluation of the frontogenesis, we also present $\hat{F}_\theta = h^{-1} \int_0^h F_\theta \, dz$, where h is a scale height for the frontal depth. The integrated frontogenesis can then be compared with the surface frontogenesis, to avoid any misleading impressions about the overall intensity or evolution of a front that might be drawn from surface data alone.

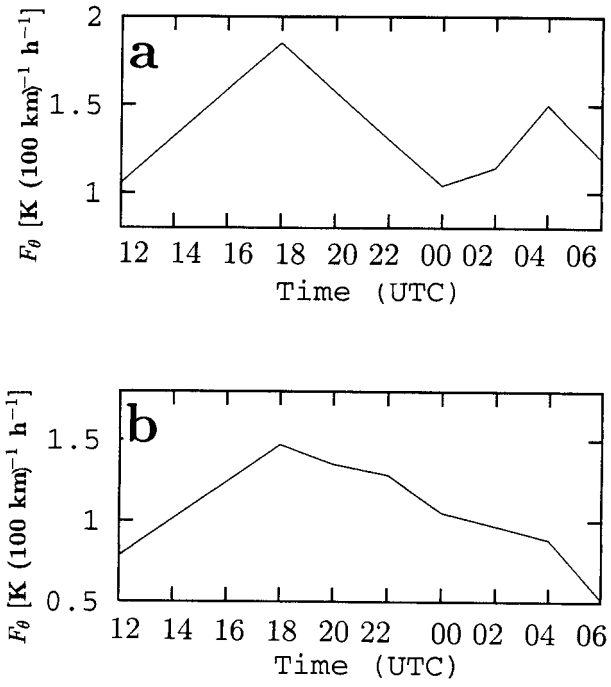

FIG. 9. Time series of (a) surface and (b) layer average vertically integrated 850 mb–surface F_θ in K (100 km)$^{-1}$ h^{-1} averaged over a portion of the frontal zone from 1200 UTC 9 Mar to 0600 UTC 10 Mar.

Figure 9 shows time evolution of the surface frontogenesis F_θ and a layer average vertically integrated frontogenesis for the period 1200 UTC 9 March to 0600 UTC 10 March. Both terms have been averaged from all model grid points in the vicinity of the most intense part of the front [defined as regions where the horizontal temperature gradient exceeds 3°C (32 km)$^{-1}$] between 37° and 44°N (except at 1200 UTC when the region was shifted northwestward to better fit the location of the front). The integrated value is a roughly 25-mb layer average determined by summing F_θ at 25-mb intervals from the surface upward through 850 mb (at most times, frontogenesis above this level was weak). The surface frontogenesis (Fig. 9a) was a maximum at 1800 UTC, local noon, when the average value was nearly 2.0 K (100 km)$^{-1}$ h^{-1}. The frontogenesis weakened after this time and became comparable to the 1200 UTC value around 0000 UTC. A secondary maximum, however, occurred in the evening when values reached 1.5 K (100 km)$^{-1}$ h^{-1} at 0400 UTC. Peak gridpoint values (figure not shown) indicated much greater variability, with one maximum in the late afternoon (2200 UTC) and a more significant maximum during the evening hours (0400–0600 UTC) when surface frontogenesis exceeded 7 K (100 km)$^{-1}$ h^{-1} in a small region as the front crossed southern Lake Michigan.

The vertically integrated frontogenesis $\hat{F}_\theta$ also reached a peak at 1800 UTC (Fig. 9b) with a much more gradual decrease than the surface frontogenesis after that time. Whereas surface frontogenesis at 0000 UTC was nearly as small as at sunrise (1200 UTC), the integrated front-

ogenesis $\hat{F}_\theta$ at 0000 UTC was still noticeably larger than at 1200 UTC. This implies a time lag between the influence of daytime diabatic effects at the surface compared with these effects in a deeper lower-tropospheric layer.

Although the data are not shown, it is worthwhile to discuss the relative roles of individual terms contributing to F_θ [see Eq. (2)]. The locations of primary positive values of these terms varied significantly. In general, the maximum values of F_θ were located near the maximum temperature gradient, with perhaps a small displacement rearward from the axis of maximum gradient. The convergence term, on average, was the largest at all times, although at most times it was opposed strongly by the relative advection term. At the surface, for instance, advection was roughly 60% as large as the convergence term at all times. The advection term was even larger relative to the convergence during the morning and early afternoon hours at higher levels, with a magnitude 80%–100% of the convergence at 850 mb at 1200 and 1800 UTC. Tilting effects were generally small, although some reasonably large positive values (roughly 20%–30% of the magnitude of the convergence term) occurred during the 1800–0000 UTC period centered at around 900 mb, or near the top of the average WCBL just behind the front. Averaged over the frontal zone, the diabatic effect was also fairly small, and near-surface values switched from frontogenetic to frontolytic by 2000 UTC. However, the diabatic term evidenced significant variations near the front, and similar to Blumen et al. (1996), was significant in some areas where it provided the largest contribution to positive frontogenesis. Areal averages may have been reduced because of the zone just behind the front where diabatic processes were frontolytic at the surface at most times, apparently the result of enhanced sensible heat flux occurring just behind the front where air temperatures fell dramatically over previously heated ground.

The time evolution of the vertical profile of F_θ in the lower troposphere can be seen in Fig. 10. Although the largest value of F_θ did occur at the surface at the latest time shown, 0600 UTC, at most other times the maximum frontogenesis was located at some level above the surface. Although the potential temperature gradient itself typically weakens with height above the surface, the increased winds at these higher levels apparently more than compensates for the weakened θ gradient in the F_θ convergence term. At many times, the largest value occurred near the top of the prefrontal WCBL, around 900 mb. The lowest values of F_θ near the surface generally occurred at 1200 UTC, with a rapid increase to the highest values at 1800 UTC. After this time, F_θ decreased fastest near the surface, and remained nearly constant through about 0000 UTC at 900 mb.

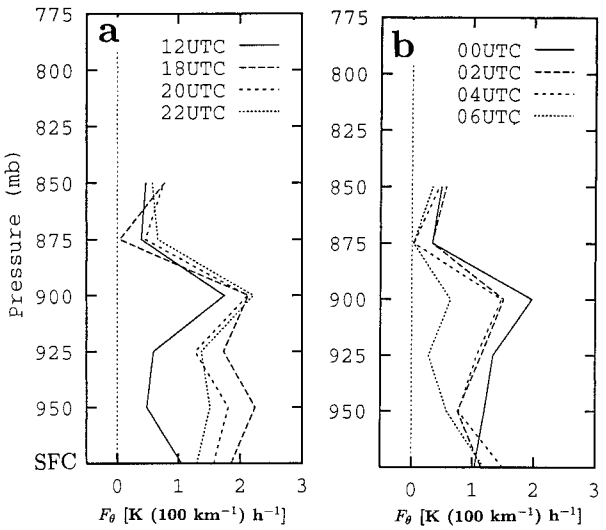

FIG. 10. Time evolution of vertical profiles of F_θ in K (100 km)$^{-1}$ h^{-1} for (a) 9 Mar at 1200 UTC, 1800 UTC, 2000 UTC, and 2200 UTC, and (b) 10 Mar at 0000 UTC, 0200 UTC, 0400 UTC, and 0600 UTC.

e. Time evolution of frontal convergence (F_u)

The time evolution of frontal convergence, F_u, can be determined using Eq. (3), and vertical profiles of the terms in this equation averaged over the frontal zone can be seen in Fig. 11. For the averaging used in this figure, the frontal zone was defined similarly to that described above for F_θ except that all points with convergence exceeding 6×10^{-5} s^{-1} were used. The different region was chosen because maximum frontal convergence in this case occurred just ahead or near the leading edge of the significant temperature gradient. Thus, the fields of F_θ and F_u are not collocated. At 1200 UTC (Fig. 11a), F_u was relatively constant with height. The convergence term and the differential pressure gradient were the largest positive contributors to F_u. Friction, relative advection, and the Coriolis term were all generally frontolytic (negative F_u) at this time. At 1800 UTC (Fig. 11b) F_u had increased at 950 mb with a pronounced maximum there. The general role of the terms was the same as at 1200 UTC, but the pressure gradient term had increased substantially, probably reflecting the influence of the differential daytime heating. The magnitude of the friction term had also increased substantially at both the surface, 950 and 925 mb due to a deepening WCBL. Only gradual changes occurred through 0000 UTC (Fig. 11c). The magnitude of frictional effects slowly decreased at low levels, as did F_u, except at the surface, where it increased slightly from 1800 UTC. The convergence term gradually strengthened during this time. During the evening (0400 UTC; Fig. 11d), total F_u continued to decrease at low levels but remained fairly constant at higher levels, with a general increase at 850 mb. The increase was primarily due to the increased convergence term. In general, the variations in F_u are fairly small, with the most pronounced feature being the general increase in the convergent tendency at the surface from 1800 UTC to a

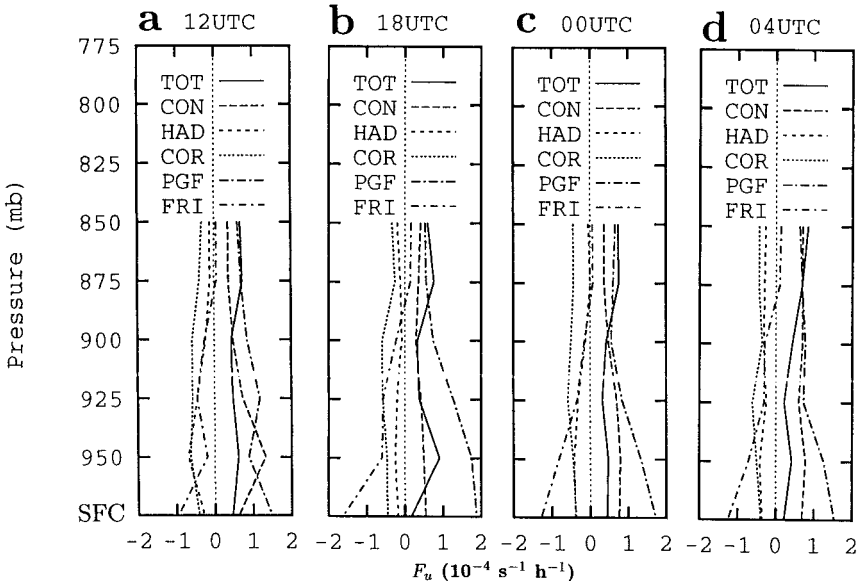

FIG. 11. Vertical profiles of total convergence tendency F_u (TOT) and contributions from convergence (CON), relative horizontal advection (HAD), Coriolis (COR), pressure gradient (PGF), and friction (FRI) terms (in 10^{-4} s^{-1} h^{-1}) during 9–10 Mar at (a) 1200 UTC, (b) 1800 UTC, (c) 0000 UTC, and (d) 0400 UTC.

peak around sunset (2200–0000 UTC) with a rapid decrease afterward.

5. Role of diabatic processes determined through 3D sensitivity tests

To further investigate the role of solar irradiance-forced diabatic heating in this frontal case, a series of simulations were performed in an effort to isolate the effect of cloud shading, surface wetness, and precipitation evaporative cooling. The first simulation to be discussed is one in which the presence of clouds was excluded from the radiation portion of the code (RAD). A second simulation was performed in which the volumetric soil moisture was decreased by 50% across the domain, to investigate both the effect on the postfrontal cloud cover (if any) and the impact of the increased warm sector sensible heat fluxes on the front evolution (DRY). Additionally, because light precipitation was occurring in the model behind the cold front, a simulation was run in which the effect of evaporative cooling of precipitation was excluded, to study the role of this diabatic process on frontal behavior (EVP). Finally, it is worth mentioning that an attempt to carry out a simulation in which condensation affects were excluded yielded unrealistic fields, and therefore this case is not considered in the sensitivity simulations.

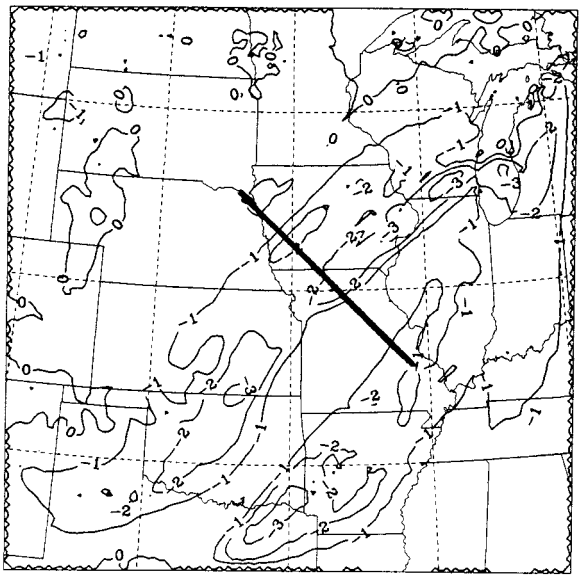

FIG. 12. Surface temperature (~70 m) difference (in K) between CTL and RAD at 2200 UTC 9 Mar. Contour interval of 1 K is used. (Solid line refers to cross sections shown in Figs. 13, 15, and 17.)

a. Cloud shading

In a simulation that excluded cloud shading impacts (beginning at 1200 UTC) on radiation reaching the surface (RAD), the frontal temperature gradient near the surface was moderately diminished, with a small decrease in frontal speed from CTL. The difference between the CTL surface air temperatures and the RAD temperatures at 2200 UTC can be seen in Fig. 12. At this time, cooling associated with cloud shading covered a broad region behind the front.

Peak cooling occurred in isolated regions, which had deviations of 3°C, in agreement with the scaling in section 2a(1). Enhanced cooling existed on the southeast

side of the more general cooled region, so that cloud-shading effects on maximum frontal temperature gradient were maximized. In general, the cloud shading intensified the frontal temperature gradient by 10%–20%.

A shallow surface cold front with a relatively *sharp* cross-front temperature difference may resemble locally a density current (e.g., Shapiro et al. 1985; Keyser 1986; Bluestein 1993). (Miller et al. 1996 observed such characteristics at the leading edge of a section of the front, which is considered in this study.) However, reservations about using the density current speed formula to determine the frontal speed have been echoed by Smith and Reeder (1988) and Koch et al. (1995). It is therefore of interest to examine the correspondence between the density current formulation estimated speed changes due to diabatic effects and the changes in simulated front speed. The speed, c, of the leading edge of a density current with a cross-current discontinuous potential temperature difference, $\Delta\theta$, and characteristic depth of the cold air sector, h, is proportional to $(h\Delta\theta)^{1/2}$. Using the density current formulation, the frontal speed should be affected by the increased gradient caused by the differential diabatic heating related to cloud shading. The 2°–3°C enhanced temperature difference should increase the frontal speed by around 10%. For this case, however, that is equivalent to an increase in movement of 1 m s^{-1}, which if constant over 12 h, should result in a difference in frontal location of around 40 km by 0000 UTC 10 March. The increased temperature contrast attributable to cloud shading, by contrast, was most significant in the afternoon. Thus, adopting the gravity current speed formulation one should expect any difference in frontal location to be on the order of 20 km or less, or no more than one model grid point. This does appear to be the case, with some evidence at a few grid points of a small increase in speed.

Figure 13 is a vertical cross section taken through the front at 2200 UTC (from north of Norfolk, Nebraska, to southeastern Missouri) showing the temperature difference between CTL and RAD (location of cross section is marked in Fig. 12). Changes in temperature were restricted to the lowest 1 km or so above ground level. The cooling due to cloud shading covers a fairly broad region. Some slight warming can be seen at around 1.6 km in height, reflecting a slightly less deep mixed layer in the control run where cloud shading occurred.

Changes in frontal temperature gradients should manifest themselves as changes in the strength of the frontal circulation, which affects low-level convergence and possibly precipitation. Both convergence and precipitation fields from this simulation (not shown) imply this to be true, with a 5% or so decrease in peak convergence along the front when cloud shading was eliminated. The impact on precipitation is more difficult to ascertain since unfavorable larger-scale conditions minimized the precipitation along the front in this case. However, in the region of strongest low-level convergence over northern Illinois, where some small amounts were simulated in the afternoon, a small but general decrease in the precipitation of up to 2 mm occurred in association with the decreased convergence in DRY compared to CTL.

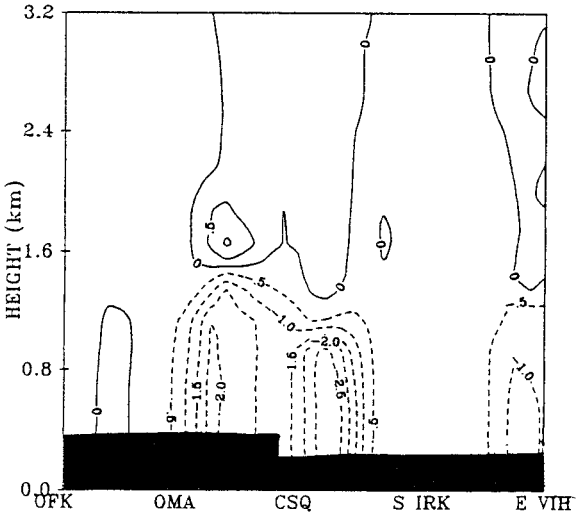

FIG. 13. Vertical cross section (see Fig. 12 for location) of temperature difference between CTL and RAD at 2200 UTC, taken perpendicular to the front from Norfolk, NE (OFK), to southeastern Missouri (E VIH). Contour interval is 0.5 K.

b. Soil moisture

To put the effects of cloud shading into perspective, an additional simulation (DRY) was run in which the initial volumetric soil moisture was reduced by 50% from the CTL run. Much of the Midwest had a volumetric soil moisture content of around 0.3 (highly wet soil) on 9 March. The reduction in soil moisture yielded volumetric soil moisture values around the soil wilting point and consequently resulted in substantial reduction in evapotranspiration. Koch et al. (1997) found that the intensity of a squall line linked to the frontal circulation in a simulated springtime case was significantly increased when a more appropriate soil moisture distribution ahead of the front, one that was drier, was used. Various studies have found that, thermodynamically, increased soil moisture is conducive to formation of convective precipitation (see, e.g., De Ridder 1997). The results of Koch et al., however, suggest that changes in dynamics may reverse the impact.

Increased sensible heat flux (accompanied by a corresponding decrease in the latent heat flux) due to the decreased soil wetness allowed for significantly more WCBL warming compared to CTL. By 1800 UTC, much of the warm sector ahead of the cold front was roughly 2°–3°C warmer than in CTL, and a slight increase in frontal speed due to an increased temperature gradient was apparent as a narrow band of cooling just northwest of the main warm sector warming (not

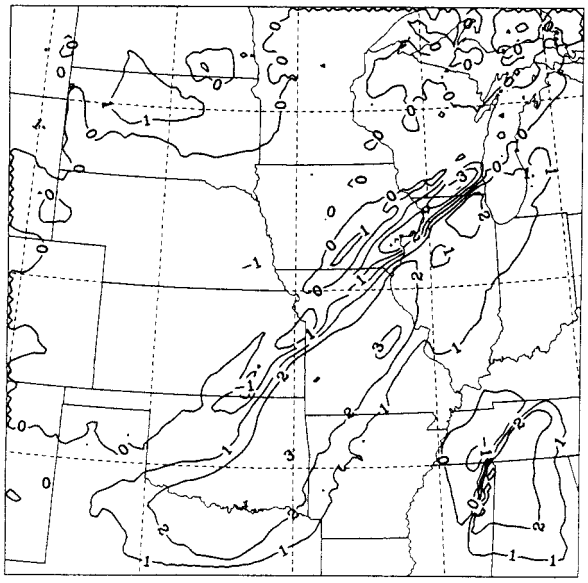

FIG. 14. As in Fig. 12 except for the difference between DRY and CTL at 2200 UTC 9 Mar.

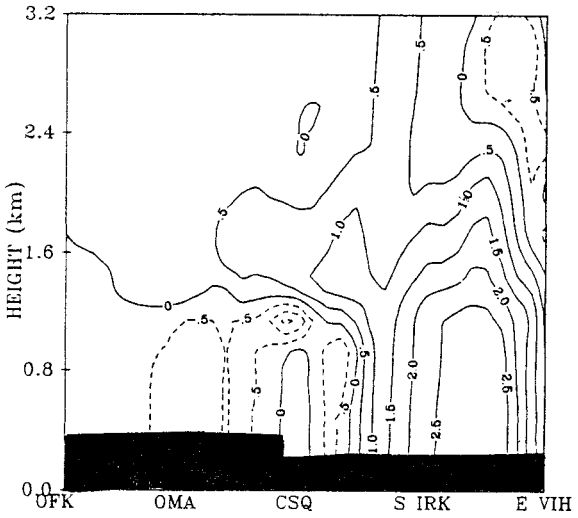

FIG. 15. As in Fig. 13 except for the difference between DRY and CTL.

shown). At 2200 UTC 9 March (Fig. 14), the increased speed of the cold front was pronounced. Warming in the warm sector was still substantial, although the peak warming occurred around 2000 UTC. A zone just ahead of the cold front had positive perturbations greater than 2°C compared to CTL. A roughly 50–100-km band with negative perturbations of 1°–3°C was evidence of the increased frontal speed. These perturbations reached 4°C at 0000 UTC. The increase in temperatures ahead of the front was generally comparable to the decrease that occurred behind the front due to cloud shading, 2°–3°C, so that the gravity current speed formulation would again predict only a 10% increase in speed. An analysis of the surface temperature field shows the actual surface front moved approximately 40 km farther to the southeast by 0000 UTC 10 March compared to the control run.

What explanation can be given for the more significant increase in front speed compared to the effect of cloud shading? Partially, some of the negative temperature departures seen in Fig. 14 were due not only to the faster speed of the front (some points experience frontal passage earlier than in CTL), but also in response to a contraction in the temperature gradient caused by a more intense cross-front circulation. The contraction should be conducive to an enhanced speed of the leading edge of the front. Additionally, however, adopting the gravity current formulation, frontal speed would also be directly proportional to the height of the layer of significant temperature gradient. Unlike the role of cloud shading, which produces a few degrees Celsius of cooling in a shallow layer near the surface, the reduction in soil wetness allows enhanced warming ahead of the front through a significantly deeper layer (see Fig. 15). The warming extended upward to nearly 3 km in the immediate vicinity of the front. The WCBL increased in height by approximately 1 km in this simulation. The greater depth of the layer of significant temperature gradient would also act to increase the frontal speed in this run. It thus appears that significant modification of soil moisture in the warm sector ahead of a cold front can have a more pronounced effect on frontal evolution than diabatic processes that might produce cooling in the cold sector. For the front simulated in this study, the gravity current formulation reasonably explains changes in the frontal movement due to diabatic effects.

c. Evaporation of precipitation

Because several studies have found that evaporation of precipitation is normally a strong diabatic process in the atmosphere, producing significant cooling rates, a simulation (EVP) was run with evaporation (of rain or snow) effects on temperature neglected. In the 9 March case, observations showed precipitation was generally absent from the immediate vicinity of the front, so that this effect should be relatively small. However, spotty light precipitation in the form of drizzle, freezing drizzle, and light snow did occur as close as 100 km behind the front with more significant steady precipitation through much of 9 March several hundred kilometers north of the front (e.g., Wang et al. 1995; Figs. 5a,b), and the evaporation of this precipitation could influence the postfrontal cold pool. The simulated precipitation fields shown in Fig. 8 appear to agree reasonably well with observations. Even small amounts of precipitation, such as the several millimeter amounts that did occur in isolated areas nearer the front, can produce substantial cooling due to the large latent heat of condensation.

Changes in the surface air potential temperature between CTL and EVP at 2200 UTC can be seen in Fig.

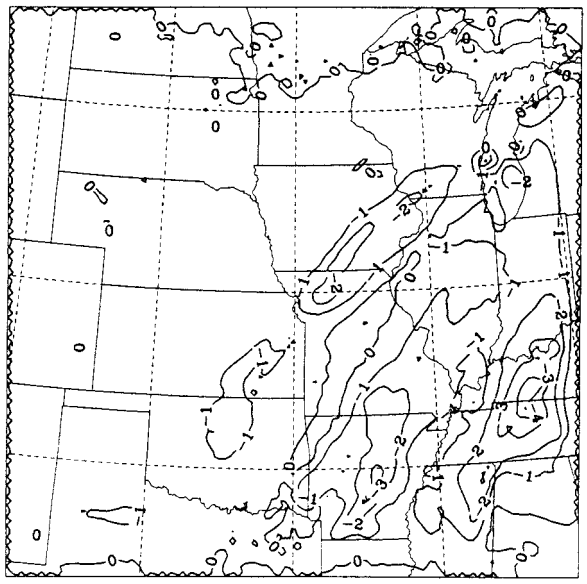

FIG. 16. As in Fig. 12 except for the difference between CTL and EVP at 2200 UTC 9 Mar.

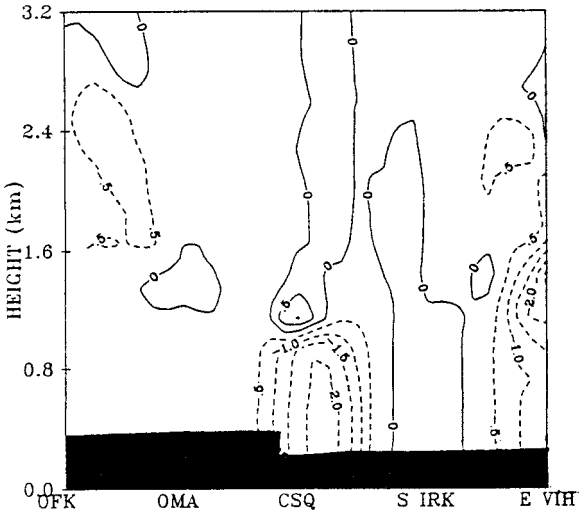

FIG. 17. As in Fig. 13 except for the difference between CTL and EVP.

16. Cooling occurred in several broad regions just behind the cold front. In general, this cooling was slightly less substantial than that associated with cloud shading, and covered a significantly smaller region. It should be noted that evaporative cooling played a more important role within the southeast portion of the warm sector where convection was occurring well ahead of the cold front.

A vertical cross section through the front (Fig. 17) showed that the cooling effect from precipitation evaporation was confined to an even more shallow layer than that associated with cloud shading. Cooling behind the front was confined to the lowest 1 km. Again some warming can be seen just above the cool perturbation, reflecting a less deep WCBL. Unlike the comparison with the no cloud shading run, there are some regions of cooling from precipitation evaporation extending to 2–3 km. These regions are disorganized and generally have little impact on the primary front. Low-level convergence was also strengthened slightly by the effect of evaporation of precipitation, but as with cloud shading, for this case there was little effect on near-frontal precipitation.

6. Discussion

The series of simulations described above isolated both the effect that reduced sensible heat flux due to cloud cover on the cold side of the front and the effect that evaporation of precipitation had on the evolution of low-level temperatures and frontal propagation. In addition, the effect of soil wetness was also examined.

To gain a better understanding of the relative importance of these processes, several measures of frontogenesis (F_θ, F_u, and F_{uq}) were computed again at several levels in the vertical for the sensitivity cases. Figure 18 shows the time evolution of the vertical profile of F_θ for the CTL, DRY, RAD, and EVP simulations. It can be seen that the deviations from the control run for each sensitivity test vary with time. Significant increases in F_θ for the DRY run generally occurred during the daylight hours with a maximum increase at 2000 UTC (Fig. 18c). The most significant increases tended to occur toward the top of the WCBL. By 0000 UTC (Fig. 18e), increases became negligible. The RAD run resulted in a reduction of F_θ during the daylight hours, with the biggest departures occurring at 1800 UTC (Fig. 18b). The impact could be as large as that associated with the dry soil, although at most times, the reduction was somewhat less than the increase that occurred with dry soil. After sunset, some increase in F_θ occurred since the removal of cloud impacts on radiation allowed the cold sector to cool faster than in the CTL run.

Unlike the DRY and RAD tests, the impact of precipitation evaporation was generally independent of time. Throughout the daylight hours the reduction in F_θ from a neglect of evaporation was similar to that from the neglect of cloud shading. During the evening, however, the reduced F_θ continued with a maximum impact at 0400 UTC (Fig. 18g). The change from the control run at this time was as large as at any time in the other sensitivity tests. In the model, more precipitation was occurring close to the front at this time than at earlier times (Fig. 8b). However, the precipitation amounts were still fairly small, suggesting that even modest precipitation can result in evaporative cooling with significant impacts on frontal temperature gradient. In this respect, the model results differ somewhat from the observational studies (e.g., Blumen et al. 1996), which emphasized the role of cloud shading, and presumed evaporative cooling, to be insignificant due to the lack

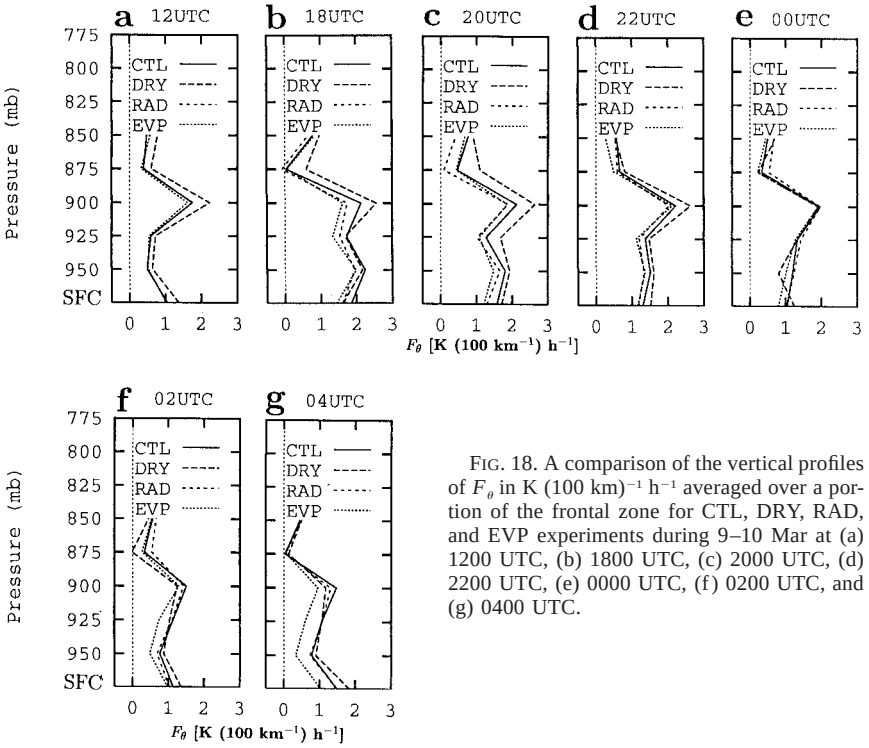

FIG. 18. A comparison of the vertical profiles of F_θ in K (100 km)$^{-1}$ h^{-1} averaged over a portion of the frontal zone for CTL, DRY, RAD, and EVP experiments during 9–10 Mar at (a) 1200 UTC, (b) 1800 UTC, (c) 2000 UTC, (d) 2200 UTC, (e) 0000 UTC, (f) 0200 UTC, and (g) 0400 UTC.

of rainfall. The difference might be partly explained by the fact that the Blumen et al. study concentrated on the period prior to 2300 UTC 9 March, and in the small region centered on or immediately adjacent to Missouri. Figure 18 implies that simulated precipitation evaporative cooling was most significant after 0000 UTC. Differences could also develop if the model overestimated the amount of precipitation falling behind the front, or produced precipitation in regions where none was observed. Figures 5a and 5b in Wang et al. (1995) generally support the model precipitation fields relatively close behind the front, although they do suggest precipitation was overestimated in the main band lying several hundred kilometers behind the front.

A comparison of F_u and F_{uq} has been done for the CTL and DRY simulations to gain insight into the interrelationship between thermodynamic and dynamic changes resulting from changes in soil moisture. As discussed earlier, drier soil conditions generally intensified both the frontal temperature gradient and the frontal circulation. Unlike the springtime case in the southeastern United States studied by Koch et al. (1997), however, little impact was simulated in DRY on the precipitation near the front. Some increase in the convergent tendency (F_u) in the dry soil run can be seen at most times during the daylight hours (Fig. 19). Of note, the largest increase was delayed until 0000 and 0200 UTC at lower levels. At this time the temperature

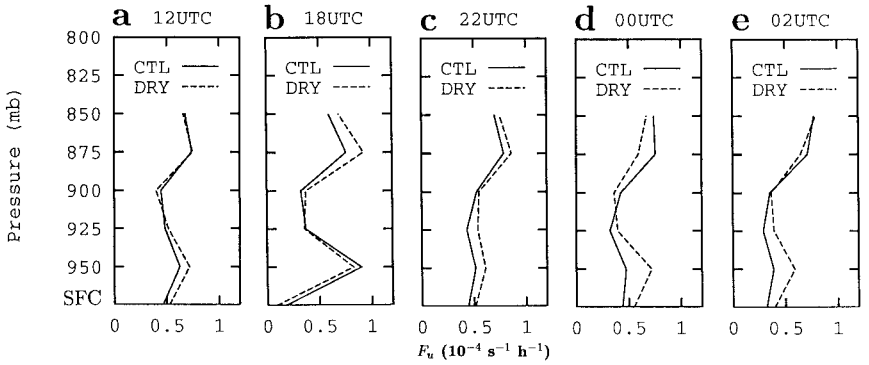

FIG. 19. Comparison of F_u in 10^{-4} s^{-1} h^{-1} between CTL and DRY simulations during 9–10 Mar at (a) 1200 UTC, (b) 1800 UTC, (c) 2200 UTC, (d) 0000 UTC, and (e) 0200 UTC.

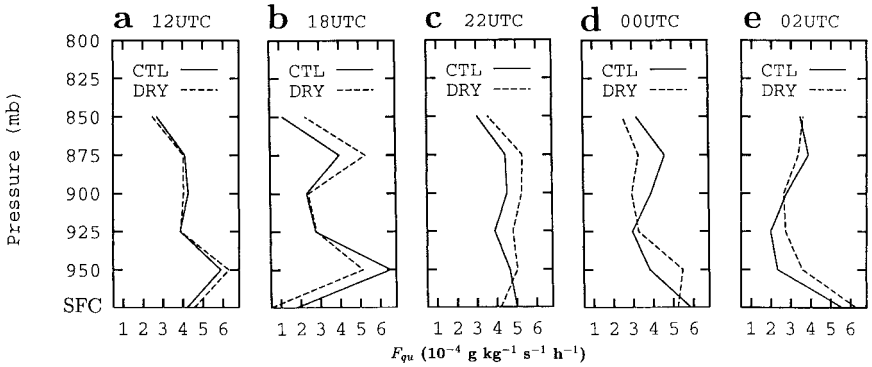

FIG. 20. As in Fig. 19 but for F_{uq} in 10^{-4} g kg^{-1} s^{-1} h^{-1}.

gradient tendency F_θ in the two runs was comparable (Fig. 18e). The increase diminished by 0400 UTC (not shown). The increased impact of the drier soil on convergence tendencies at 0000 and 0200 UTC (Figs. 19c,d) may be evidence of the dynamic impact of an increased WCBL depth.

Vertical profiles of F_{uq} can be seen in Fig. 20. The time tendency of moisture convergence along the front may be the best quantity to determine which effect, thermodynamic or dynamic, is of greatest importance. An evaluation of all the terms in Eq. (4) (figure not shown) finds that the first term is significantly larger than all of the others. Thus, moisture convergence tendencies were influenced strongly by flow convergence tendencies. Relative advection of the moisture gradient, and differential moistening in the cross-front direction, occasionally also contributed to increasing moisture convergence, with magnitudes typically no more than 5%–20% of the first term. However, relative advection played a much more important role around 900 mb from 2000 UTC through 0200 UTC when its magnitude reached 30%–80% of that of the first term.

In the dry soil run, F_{uq} is reduced near the surface at all times (after 1200 UTC) except for 0200 UTC (Fig. 20e). Thus the thermodynamic impact is overriding the improved dynamic effect seen in F_u (Fig. 18). Above the surface, however, the moisture convergence tendency is generally greater in the dry soil run at most times. Around 0000 UTC (Fig. 20d), there is a layer above 925 mb where the moisture convergence tendency decreases in the dry soil case; however, below 925 mb, the tendency increases as at other times. The integrated effect generally appears to favor more moisture convergence, especially during the late afternoon and early evening hours. Although the 9 March case lacked sufficient larger-scale thermodynamics for significant frontal precipitation, the tendency to increase integrated moisture convergence with drier soil agrees with that found in the case modeled by Koch et al. (1997). However, the relationship between precipitation and soil moisture may be very sensitive to background conditions, and caution must be used in generalizing the results from only two cases.

7. Conclusions

The impact of diabatic heating or cooling on frontal evolution has been investigated using high-resolution simulations of a dry front case that occurred in the midwestern United States during STORMFEST 1992. Conceptual evaluations suggest that cloud shading can measurably influence frontal evolution in the late winter period, as argued in the observational studies of this event by Miller et al. (1996) and Blumen et al. (1996). In addition, evaporation of precipitation results in cooling that may comparably influence front evolution. For weak fronts, these diabatic effects may become more significant.

Soil moisture has been shown to impact frontal precipitation (Koch et al. 1997), but conceptual evaluations suggest the effects may involve a complex interaction between thermodynamic changes in the lower troposphere and dynamic changes. Drier soil increases surface sensible heat flux, which intensifies frontal temperature gradients in cases where cloud cover is restricted to the cold side of a front. Dry soil may also increase the frontal convergence and could alter the frictionally influenced inertial oscillation, potentially increasing frontal strength for a period during the nighttime hours.

Sensitivity simulations for this case found that cloud shading and precipitation evaporation played generally comparable roles in increasing the frontal temperature gradient and circulation during the daylight hours. Both processes maintained colder air in the cold sector, and the increased temperature gradient resulted in some increase in frontal speed, as implied by density current theory. A reduction in soil moisture increased the sensible heat flux in the warm sector, significantly increasing the frontal temperature gradient. Although increases in the traditional frontogenesis term (F_θ) were similar to the decreases experienced in the simulation without cloud shading, the impact on frontal speed was greater, and the temperature changes from the control run occurred through a deeper layer. Overall, the gravity current speed formula generally estimated well the changes in the simulated frontal speed. Drier soil also resulted

in an increase in the convergence tendency along the front, a sign of the positive dynamic effect on frontal intensity. Moisture convergence tendency, however, was reduced at the surface indicating the dominating negative effect of reduced evapotranspiration on the thermodynamic environment. Through a deeper layer above the surface, however, moisture convergence was noticeably larger with drier soil, implying that the dynamic changes were of greater significance than the reduced latent heat flux associated with drier soil.

Acknowledgments. The authors would like to thank Prof. George Kallos and his group at the University of Athens, Greece, for providing the work station Eta Model and for assistance in its implementation at Iowa State. Additional thanks are given to Drs. Eric Rogers and Tom Black, and Mike Baldwin at NCEP for providing a few fields necessary for running the model, and to Tianshi Li for assistance with some figures. The constructive comments of two anonymous reviewers were appreciated. This work was sponsored by the National Science Foundation/National Oceanic and Atmospheric Administration Grant ATM-9612388 in the USWRP program. This is Journal Paper J-17975 of the Iowa Agricultural and Home Economics Experiment Station, Ames, Iowa, Projects 3435 and 3245, supported by Hatch Act and State of Iowa funds.

REFERENCES

Betts, A. K., 1986: A new convective adjustment scheme. Part I: Observational and theoretical basis. *Quart. J. Roy. Meteor. Soc.*, **112,** 677–692.

——, and M. J. Miller, 1986: A new convective adjustment scheme. Part II: Single column tests using GATE wave, BOMEX, and arctic air-mass data sets. *Quart. J. Roy. Meteor. Soc.*, **112,** 693–709.

Bluestein, H. B., 1993: *Synoptic-Dynamic Meteorology in Midlatitudes.* Vol. 2. Oxford University Press, 594 pp.

Blumen, W., N. Gamage, R. L. Grossman, M. A. LeMone, and L. J. Miller, 1996: The low-level structure and evolution of a dry arctic front over the central United States. Part II: Comparison with theory. *Mon. Wea. Rev.*, **124,** 1676–1692.

Businger, S. W., H. Bauman III, and G. F. Watson, 1991: The development of the Piedmont front and associated outbreak of severe weather on 13 March 1986. *Mon. Wea. Rev.*, **119,** 2224–2251.

Chen, F., K. Mitchell, J. Schaake, Y. Xue, H.-L. Pan, V. Koren, Q. Y. Duan, M. Ek, and A. Betts, 1996: Modeling of land surface evaporation by four schemes and comparison with FIFE observations. *J. Geophys. Res.*, **101,** 7251–7277.

De Ridder, K., 1997: Land surface processes and the potential for convective precipitation. *J. Geophys. Res.*, **102,** 30 085–30 090.

Eliassen, A., 1962: On the vertical circulation in frontal zones. *Geophys. Publ.*, **24,** 147–160.

Gallus, W. A., Jr., and R. H. Johnson, 1995: The dynamics of circulations within the stratiform regions of squall lines. Part I: The 11 June PRE-STORM system. *J. Atmos. Sci.*, **52,** 2161–2187.

Garratt, J. R., 1992: *The Atmospheric Boundary Layer.* Cambridge University Press, 316 pp.

——, and W. L. Physick, 1987: Numerical study of atmospheric gravity currents. Part II: Evolution and external influences. *Beitr. Phys. Atmos.*, **60,** 88–102.

Gerrity, J. P., T. L. Black, and R. E. Treadon, 1994: On the numerical solution of the Mellor–Yamada level 2.5 turbulent kinetic energy equation in the Eta Model. *Mon. Wea. Rev.*, **122,** 1640–1646.

Hamilton, R. A., and J. W. Archbold, 1945: Meteorology of Nigeria and adjacent territory. *Quart. J. Roy. Meteor. Soc.*, **71,** 231–265.

Holtslag, A. A., and M. Ek, 1996: Simulation of surface fluxes and boundary layer development over the pine forest in HAPEX–MOBILHY. *J. Appl. Meteor.*, **35,** 202–213.

Janjic, Z. I., 1994: The step-mountain Eta coordinate model: Further developments of the convection, viscous sublayer, and turbulence closure schemes. *Mon. Wea. Rev.*, **122,** 927–945.

Keyser, D., 1986: Atmospheric fronts: An observational perspective. *Mesoscale Meteorology and Forecasting,* P. Ray, Ed., Amer. Meteor. Soc., 216–258.

Koch, S. E., T. McQueen, and V. M. Karyampudi, 1995: A numerical study of the effects of differential cloud cover on cold frontal structure and dynamics. *J. Atmos. Sci.*, **52,** 937–964.

——, A. Aksakal, and J. T. McQueen, 1997: The influence of mesoscale humidity and evapotranspiration fields on a model forecast of cold-frontal squall line. *Mon. Wea. Rev.*, **125,** 384–409.

Lin, C. A., and R. E. Stewart, 1991: Diabatically forced mesoscale circulations in the atmosphere. *Advances in Geophysics,* Vol. 33, Academic Press, 267–305.

Lobocki, L., 1993: A procedure for the derivation of surface-layer bulk relationships from simplified second-order closure models. *J. Appl. Meteor.*, **32,** 126–138.

Martin, J. E., J. D. Locatelli, P. V. Hobbs, P.-Y. Wang, and J. A. Castle, 1995: Structure and evolution of winter cyclones in the central United States and their effects on the distribution of precipitation. Part I: A synoptic-scale rainband associated with a dryline and lee trough. *Mon. Wea. Rev.*, **123,** 241–263.

Mellor, G. L., and T. Yamada, 1974: A hierarchy of turbulence closure models for planetary boundary layers. *J. Atmos. Sci.*, **31,** 1791–1806.

——, and ——, 1982: Development of a turbulence closure model for geophysical fluid problems. *Rev. Geophys. Space Phys.*, **20,** 851–875.

Mesinger, F., Z. I. Janjic, S. Nickovic, D. Gavrilov, and D. G. Deaven, 1988: The step mountain coordinate: Model description and performance for cases of alpine cyclogenesis and for a case of an Appalachian redevelopment. *Mon. Wea. Rev.*, **116,** 1493–1518.

Miller, J. E., 1948: On the concept of frontogenesis. *J. Meteor.*, **5,** 169–171.

Miller, L. J., M. A. LeMone, W. Blumen, R. L. Grossman, M. Gamage, and R. Zamora, 1996: The low-level structure and evolution of a dry arctic front over the central United States. Part I: Mesoscale observations. *Mon. Wea. Rev.*, **124,** 1648–1675.

Noilhan, J., and S. Planton, 1989: A simple parameterization of land surface processes for meteorological models. *Mon. Wea. Rev.*, **117,** 536–549.

Oliver, V. J., and G. C. Holzworth, 1953: Some effects of the evaporation of widespread precipitation on the production of fronts and on changes in frontal slopes and motions. *Mon. Wea. Rev.*, **81,** 141–151.

Pan, H.-L., and L. Mahrt, 1987: Interaction between soil hydrology and boundary-layer development. *Bound.-Layer Meteor.*, **38,** 185–202.

Sanders, F., 1955: An investigation of the structure and dynamics of an intense surface frontal zone. *J. Meteor.*, **12,** 542–552.

Sawyer, J. S., 1956: The vertical circulation at meteorological fronts and its relation to frontogenesis. *Proc. Roy. Soc. London,* **A234,** 346–362.

Segal, M., W. L. Physick, J. E. Heim, and R. W. Arritt, 1993: The enhancement of cold front temperature contrast by differential cloud cover. *Mon. Wea. Rev.*, **121,** 867–873.

Shapiro, M. A., T. Hampel, D. Rotzoll, and F. Mosher, 1985: The frontal hydraulic head: A micro-α scale ($\sim$1 km) triggering mechanism for mesoconvective systems. *Mon. Wea. Rev.*, **113,** 1166–1183.

Smith, R. K., and M. J. Reeder, 1988: On the movement and low-level structure of cold fronts. *Mon. Wea. Rev.*, **116,** 1927–1944.

U.S. Department of Energy, 1981: *Solar Radiation Energy Atlas of the U.S.* SERI/SP-642-1037, 167 pp. [Available from Superintendent of Documents, U.S. Government Printing Office, Washington, DC 20402.]

Wang, P.-Y., J. E. Martin, J. Locatelli, and P. Hobbs, 1995: Structure and evolution of winter cyclones in the central United States and their effects on the distribution of precipitation. Part I: A synoptic-scale rainband associated with a dryline and lee trough. *Mon. Wea. Rev.*, **123,** 241–264.

Ye, Z. J., M. Segal, J. R. Garratt, and R. A. Pielke, 1989: On the impact of cloudiness on the characteristics of nocturnal downslope flows. *Bound.-Layer. Meteor.*, **49,** 23–51.

Zhao, Q., F. H. Carr, and G. B. Lesins, 1991: Improvement of precipitation forecasts by including cloud water in NMC's Eta Model. Preprints, *Ninth Conf. on Numerical Weather Prediction*, Denver, CO, Amer. Meteor. Soc., 50–53.